Journal of Colloid and Interface Science 584 (2021) 57–66

Contents lists available at ScienceDirect

Journal of Colloid and Interface Science

journal homepage: www.elsevier.com/locate/jcis

Regular Article

PEDOT:PSS nano-particles in aqueous media: A comparative experimental and molecular dynamics study of particle size, morphology and z-potential

Karishma Jain [a,1], Aleksandar Y. Mehandzhiyski [c,1], Igor Zozoulenko [c,d,*], Lars Wågberg [a,b,*]

[a] Department of Fibre and Polymer Technology, KTH Royal Institute of Technology, Teknikringen 56, SE-100 44 Stockholm, Sweden
[b] Wallenberg Wood Science Center, KTH Royal Institute of Technology, Teknikringen 56, SE-100 44 Stockholm, Sweden
[c] Laboratory of Organic Electronics, Department of Science and Technology (ITN), Campus Norrköping, Linköping University, 60174 Norrköping, Sweden
[d] Wallenberg Wood Science Center, Linköping University, SE-60174 Norrköping, Sweden

GRAPHICAL ABSTRACT

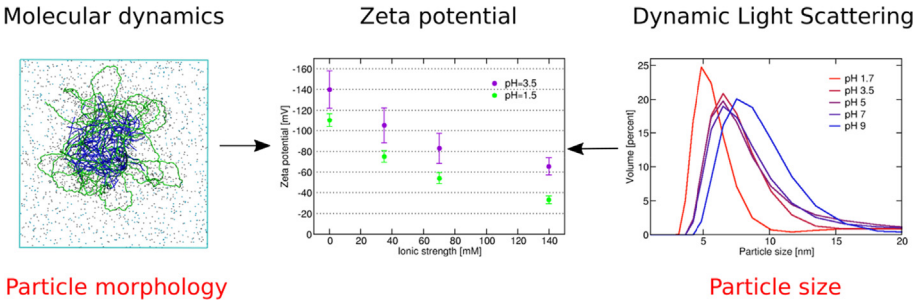

ARTICLE INFO

Article history:
Received 16 July 2020
Revised 16 September 2020
Accepted 17 September 2020
Available online 24 September 2020

Keywords:
PEDOT:PSS
Molecular dynamics simulations
Particle morphology
Zeta potential
Dynamic light scattering
Charge density

ABSTRACT

PEDOT:PSS is the most widely used conducting polymer in organic and printed electronics. PEDOT:PSS films have been extensively studied to understand the morphology, ionic and electronic conductivity of the polymer. However, the polymer dispersion, which is used to cast or spin coat the films, is not well characterized and not well understood theoretically. Here, we study in detail the particle morphology, size, charge density and zeta potential (z-potential) by coarse-grained MD simulations and dynamic light scattering (DLS) measurements, for different pH levels and ionic strengths. The PEDOT:PSS particles were found to be 12 nm–19 nm in diameter and had a z-potential of −30 mV to −50 mV when pH was changed from 1.7 to 9, at an added NaCl concentration of 1 mM, as measured by DLS. These values changed significantly with changing pH and ionic strength of the solution. The charge density of PEDOT:PSS particles was also found to be dependent on pH and ionic strength. Besides, the distribution of different ions (PSS^-, $PEDOT^+$, Na^+, Cl^-) present in the solution is simulated to understand the particle morphology and molecular origin of z-potential in PEDOT:PSS dispersion. The trend in change of particle size, charge density and z- potential with changing pH and ionic strength are in good agreement between the simulations and experiments. Our results show that the molecular model developed in this work represents very well the PEDOT:PSS nano-particles in aqueous dispersion. With this study, we hope to provide new insight and an in-depth understanding of the morphology and z-potential evolution in PEDOT:PSS dispersion.

* Corresponding authors at: Laboratory of Organic Electronics, Department of Science and Technology (ITN), Campus Norrköping, Linköping University, 60174 Norrköping, Sweden (I. Zozoulenko). Department of Fibre and Polymer Technology, KTH Royal Institute of Technology, Teknikringen 56, SE-100 44 Stockholm, Sweden (L. Wågberg).
E-mail addresses: igor.zozoulenko@liu.se (I. Zozoulenko), wagberg@kth.se (L. Wågberg).
[1] These authors contributed equally to the present work.

https://doi.org/10.1016/j.jcis.2020.09.070
0021-9797/

1. Introduction

The conductive PEDOT: PSS polymer complex is scientifically important and one of the most commonly used conducting polymer in organic and printed electronics [1]. Due to its ease of solution processability, high conductivity, chemical and thermal stability, it is widely used in energy conversion and energy storage devices [2]. The polymer is available as a water stable colloidal dispersion of PEDOT (poly(3,4-ethylenedioxythiophene)) polymerized in presence of excess anionic polyelectrolyte PSS (poly styrene sulfonate), which acts as both counterion and a stabilizer [3].

Experimental techniques such as X-ray and UV photoelectron spectroscopy [4,5], X-ray scattering and diffraction studies [6,7], AFM and STM [8–10], have earlier been employed to study the structure and morphology of PEDOT:PSS thin films. Different models have been proposed for the organisation of the polymers inside the complex and in materials formed from these complexes, based on these techniques. In general, the consensus is a core shell structure of the PEDOT:PSS complexes where conductive PEDOT crystallites form the core surrounded by a shell of excess PSS. Since PSS is insulating, secondary dopants such as ethylene glycol or DMSO [8,11] are commonly used to improve the conductivity of the final PEDOT:PSS films. A comprehensive understanding of PEDOT:PSS self-association under different conditions have largely been derived from studying spin coated films. Although, PEDOT:PSS films were intensively studied, the dispersion of PEDOT:PSS is, to the knowledge of the authors, surprisingly poorly understood. It could be due to the inherent difficulty in the tedious characterization of nano-particles in dispersion and that the community using the conducting polyelectrolyte complex is less focused on characterising nanoparticles and their colloidal properties. The commercially available dispersion, Clevios PH1000, contains 30 nm PEDOT: PSS colloidal gel particles according to the manufacturer. Traditionally, Dynamic Light scattering (DLS) techniques are commonly used to measure size of colloidal particles. In previous studies, the particle size of PEDOT:PSS was reported to vary between 30 nm – 1 μm [12–14]. Moreover, the properties of the polyelectrolyte complex is rather ill-defined and conditions such as pH, ionic strength, sample preparation etc. and which techniques that have been used to measure the particle size are not always defined. There are nevertheless a few studies on the effect of pH on conductivity and performance of PEDOT:PSS films but not on the colloidal behaviour of the PEDOT:PSS dispersion, as such [15,16]. In order to be able to forecast the properties of PEDOT:PSS complexes in dispersion it is necessary to meticulously study the effect of solution parameters such as pH and ionic strength on the structural changes of the particles, and understand how different changes in solution properties affect the stability of the particles and the interaction between the PEDOT:PSS and different carrier materials [17–19].

To the knowledge of the authors there is neither common view on the properties of PEDOT:PSS complexes in aqueous media nor any accepted protocols for characterizing these properties. This can partly be attributed to the lack of theoretical studies of PEDOT:PSS complexes. Previously, all atomistic and coarse-grained molecular dynamics simulations have been used to develop theoretical models for tosylate-doped PEDOT and PEDOT:PSS films [20–24]. However, due to the complexity of the polymer structure of PEDOT:PSS, the theoretical studies of morphology of PEDOT:PSS particles are sparse [23,24]. To the best of our knowledge, only thin films of PEDOT:PSS have been studied, while the PEDOT:PSS particles in dispersion and the microscopic origin of zeta potential (z-potential) in such dispersions have not been studied theoretically or by simulations.

In this study, a microscopic model has been developed using coarse-grained molecular dynamics simulation to describe the properties of the polyelectrolyte complex to obtain spatial distribution of PEDOT, PSS, Na^+ and Cl^- ions in the solution. In addition, z-potential and particle size are calculated based on these models. In conjunction with the molecular dynamics simulations, DLS has been used to study the particle size and z-potential of PEDOT:PSS complexes. The pH and ionic strength were altered both experimentally and computationally to study the change in properties of the PEDOT:PSS particles. We are convinced that the results from the present study will provide a foundation for theoretical and experimental understanding of different factors affecting morphology, z-potential and colloidal properties of PEDOT:PSS complexes in solution.

2. Model description

2.1. Coarse-grained model

In order to model the properties of the PEDOT:PSS particles in dispersion, the MARTINI [25] coarse-grained (CG) force field was used to build the PEDOT and PSS polymer chains. The MARTINI CG force field groups on average 4 heavy atoms (C, O, N, S etc.) into 1 interaction bead and therefore reduces the overall computational power needed to evaluate the forces between the atoms. At the same time, it has been demonstrated that it can reproduce very well morphology and atomistic structures of many different systems including PEDOT and PSS [20,23–25]. The MARTINI model of Vögele et al. [26] was used earlier to model the PSS chains in PEDOT:PSS thin film [23], and it was also used in the present work. PEDOT was modelled with the recently developed MARTINI model by Modarresi et al. [20] In this model, every EDOT monomer is charged (+0.333e), which corresponds to a typical experimental oxidation level of 33% [22,27]. The length of PEDOT chains is estimated to be 10–20 monomer units [21,27]. In our calculations, we use the degree of polymerization DP = 12, and therefore the total charge of a single PEDOT chain is +4e. Both PSS and PEDOT structures with their corresponding CG mapping, are presented in Fig. 1a. The standard MARTINI (non-polarizable) models were used for Na^+ and Cl^- where each ion is represented by positive/negative sphere (CG bead) with charge +1 and –1, respectively [25]. The ion models in MARTINI represent the ion together with its first solvation shell of water surrounding the ion. We used the polarizable water model for MARTINI, which consists of three beads and corresponds to four water molecules [28].

2.2. Systems description and simulation protocol

As was mentioned earlier, the PEDOT synthesized in the presence of PSS is commercially available as a stable dispersion both due to a high surface charge and hence a high zeta potential [27,29,30]. The PSS chains extending from the complex surface likely act as a steric stabilizer upon closer contact between the complexes. To prepare highly conductive dried films, the PEDOT:PSS dispersion is usually spin coated followed by solvent evaporation [27,30].

To model PSS chain we used the degree of polymerization DP = 2200 corresponding to a typical experimental value of PSS used in the complex [31]. We also used a computationally simple model, where instead of one long polymer chain we used several (22) shorter chains with DP = 100. Note that in both models, we have the same number of PEDOT molecules and styrene sulfonate monomers, and it corresponds to PEDOT:PSS ratio of 1:2.5, i.e. typical commercial sample ratio. Our simulations demonstrated that both models give very similar results. It should be noted however, that we did not know *a priori* what particle size we would obtain with this particular number of molecules that were considered in the simulations. The results presented in the main text correspond

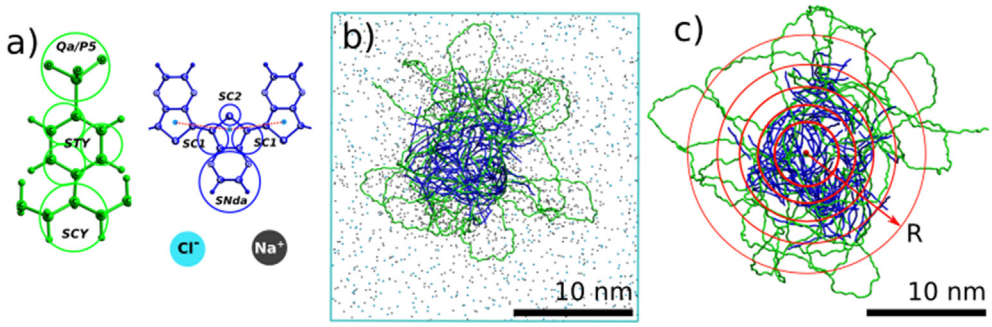

Fig. 1. (a) Chemical structures of PEDOT and PSS. The circles show the atoms which are grouped in the same coarse-grained bead together with their respective name within the MARTINI model. (b) Simulation snapshot of the PEDOT:PSS complex in dispersion; water molecules are not displayed for clarity and Na^+ and Cl^- ions are shown as dots. (c) Schematic illustration of a division of the particle into shells with radius R, where the red dot corresponds to the centre of mass of the particle. (For interpretation of the references to colour in this figure legend, the reader is referred to the web version of this article.)

to the model with one PSS chain constituting a PEDOT:PSS particle, while the results for the second model are presented in the appendix (see Fig. S1).

Since PEDOT is mainly hydrophobic and PSS is mainly hydrophilic, (due to the charged groups), in the beginning of simulations, PEDOT is placed in the centre of the particle and is surrounded by PSS, see Figs. 1 and S2. It should however be noted, that part of the PSS chain also penetrates into the dense PEDOT core. The particles are solvated with water, and Na^+ and Cl^- ions are then added to the system. The PEDOT:PSS content in the simulation box is around 5 wt%, which is close to a typical value of commercially available PEDOT:PSS dispersions [30]. PSS is assigned an average pK_a around 1.5 (since the change of pK_a -value with the surface potential of the polyelectrolyte was beyond the scope of this initial investigation) [32], and therefore it is fully deprotonated in the dispersion of the commercial products, which usually has a pH value of around 3.5. We prepared two systems, one where all the sulfonate groups were deprotonated and a second one where half of the sulfonate groups were protonated and half deprotonated. These two cases correspond to pH levels above and around the pK_a of PSS, (pH = 3.5 and pH = 1.5 respectively). It should be noted that in the case of coarse-grained MARTINI simulations, the protonated and deprotonated groups differ by the bead type, therefore by different charge and the Lennard-Jones parameters. The deprotonated sulfonate group carries negative charge (q = −1), hence, it is modelled with the Qa Martini bead, while the protonated (neutral) group is modelled with the polar type bead P5 [23], see Fig. 1a. We have chosen to randomly protonate the sulfonate groups in the case with the lower pH. We also investigate the effect of the ionic strength on the zeta potential, and therefore we prepared four cases with salt concentrations 0, 35, 70, 140 mM NaCl. In total we have investigated 16 systems (i.e. four salt concentrations, two pH = 1.5, 3.5 and two models of PSS chains with DP = 2200 and 100). We have run three independent simulations (different realizations with different initial conditions) for all the systems mentioned above. Simulation snapshots of the initial structures and the number of species in the different systems can be found in the Supporting Information Fig. S2 and Table S1, respectively.

The systems were initially minimized with the conjugated gradient method, followed by 100 ps water equilibration, where position restraints were applied on the PEDOT and PSS. After that, rescaling of the box was carried out with the NPT ensemble (constant Number of particles, Pressure and Temperature) for 200 ps and finally an equilibration at 1 bar and 300 K was carried out for 2 ns in the NPT ensemble. Finally, 50 ns production run was carried out in the NPT ensemble at 1 bar and 300 K. The trajectories were saved every 100 ps and for the calculation of all the results we used the last 40 ns of the production run, and therefore 400 frames in total. The additional two independent simulations (different realizations, as explained above) were prepared by applying simulated annealing procedures for 100 ns followed again by equilibration and production runs. In the simulated annealing procedure, the temperature was increased linearly from 300 K to 600 K and then decreased again to 300 K. The Berendsen barostat [33] with isotropic coupling and the velocity rescaling thermostat [34] were used to control the pressure and the temperature, respectively. The coupling constants for the barostat and the thermostat were set to 10 ps and 2 ps, respectively. The Particle Mesh Ewald (PME) method [35] for the long-range electrostatic interactions with the cut-off of 1.2 nm was used. The cut-off of the van der Waals interactions was also set to 1.2 nm. With the coarse-grained representation of water in MARTINI, it is necessary to use a background electrical permittivity, which is set to $\varepsilon_r = 2.5$ in the case of polarizable water model [28]. All molecular dynamics simulations were performed with the GROMACS-v2018 simulation package [36]. The simulation snapshots were prepared with VMD [37] and the analysis of the MD trajectories was done with the MDAnalysis python library [38,39].

2.3. Electrostatic potential calculations

To calculate the electrostatic potential generated by structure of the formed PEDOT:PSS particles, we assumed a spherical geometry of the particle as shown in Fig. 1c. First, the centre of mass (COM) of the particle, considering all PEDOT and PSS atoms, is determined for every frame of the simulation trajectory. Second, the particle is divided into spherical shells with a bin width of d = 2.5 Å, where the probability distributions of PEDOT, PSS, Na^+, Cl^- and charge distributions are calculated. Finally, the electric field $E(r)$ is calculated from the total charge distribution enclosed inside Gaussian spheres with radius R, with respect to the COM of the particle:

$$E(r) = \frac{1}{4\pi\varepsilon_0\varepsilon_r}\frac{q}{r^2} \tag{1}$$

where q is the total charge inside a sphere with radius r measured from the COM of the particle; ε_0 and ε_r are vacuum permittivity and relative permittivity, respectively. We used $\varepsilon_r = 78{,}4$ which corresponds to water at 298 K [40]. The electrostatic potential is then calculated using its definition by integrating the electric field:

$$V(r) = \int_r^{\infty} E(r)dr \tag{2}$$

where the upper limit of integration is in practice limited by the simulation box. Note that the water molecules are not implicitly

included in the calculation of the electric field, because they contribute to it implicitly, via the dielectric constant ε_r.

3. Experimental materials and methods

3.1. Sample preparation

1.3 wt% dispersion of PEDOT: PSS (Heraeus Clevios pH 1000, 1:2.5) was diluted to 0.1 wt%, set to pH 3.5 and dialyzed for three days. The dialyzed sample was further diluted to a concentration of 0.5 g/l, filtered through 0.45 μm syringe filter, to remove dust and big aggregates. HCl or NaOH was used to set pH and 1 M NaCl was used to set the ionic strength of the PEDOT: PSS solution. All the samples were prepared in 1 mM NaCl unless otherwise specified. Subsequently, the counterions in PEDOT: PSS solution was exchanged to protons by dialyzing at pH 1. The ionic strength and pH used in this study are 1 mM, 5 mM, 10 mM, 50 mM; pH: 1.7, 3.5, 5, 7, 9. For the lowest added salt concentration, 1 mM NaCl, the influence of the PEDOT:PSS particles will affect the total ionic strength and this is also the case for the adjustment to the lowest pH level with HCl.

3.2. Dynamic Light Scattering (DLS)

The particle size (presented as diameter) and zeta potential measurements were performed using dynamic light scattering (DLS) (Zetasizer ZEN3600, Malvern Instruments Ltd. U.K.). In this configuration, a back-scattering detector is used. Disposable folded capillary cells were used for size as well as zeta potential analysis. The measurements were repeated two times with 50 runs per measurement.

3.3. Polyelectrolyte Titration (PET)

The surface charge density of PEDOT: PSS was measured at different pH (with added 1 mM NaCl) by titrating with PDADMAC (poly (diallydimethylammonium chloride)) using a Stabino polyelectrolyte titrator (Particle Matrix GmBH, Germany). The measurements were repeated 3 times for each set to calculate the charge density in μeq/g.

4. Results and discussion

4.1. Particle morphology seen through the computational microscope

Molecular simulations can provide an invaluable insight into the structure of materials, which is why they are often referred to as a computational microscopy [41,42]. The charge distribution (probability) functions of the different species (PEDOT, PSS, Na^+, Cl^-) with respect to the centre of mass (COM) for NaCl concentration of 140 mM and pH 3.5 and 1.5 are presented in Fig. 2a and 2b, respectively. The radial distribution functions for the second particle model (DP = 22 for PSS), can be found in Figs. S1 and S3 in the Supporting Information. In the distributions presented in Fig. 2 a,b, it can be clearly seen that PEDOT occupies the inner region spanning up to around 8 nm. PSS forms a shell with thickness of about 4 nm around PEDOT. In both cases, PSS distribution expands to around 12–13 nm. Na^+ ion distribution is found to overlap with PSS due to the compensation of the negative PSS charges. The maximum of the Cl^- distribution is, as expected, found to be outside the particle. The PEDOT:PSS particles, therefore, resemble the soft particle model [43–46], with the dense PEDOT core surrounded by a shell of PSS, and Na^+ ions situated inside the PSS shell. In light of this model, the position of the slipping plane defining the zeta-potential, and to a large extent the particle size, is expected to be around the end of the extended chains forming the soft shell [43]. It should be noted that in Fig. 2b, it can be seen that PSS chains extend up to 16 nm, which is due to the non-uniformity of the particle where only a small part of the chain extends outside from the particle, see Fig. 1b for a representative illustration. Therefore, the major part (95% of the distribution) of PSS is limited to a sphere of the radius of around 12–13 nm. We can, hence, conclude from the radial distributions presented from Fig. 2a and 2b, that the particle diameter of the simulated particles is 25–26 nm, based on the observation that the distribution of PSS extend to 12–13 nm in the radial direction.

Furthermore, as seen from Figs. 1b,c and 2a,b, there is a considerable extension of the PSS out from the core of the complex and this induces both an electrostatic and steric contributions to the colloidal stability of the complex. As the pH is decreased, it can also be noted that the complex assumes a more compact structure and the Na^+ concentration is significantly decreased within the complex as expected, and the present model allows for a quantification of the Na^+ concentrations when the pH level changes. The radial distributions of PSS presented in Fig. S3c show the particle is smaller for lower pH. This is due to the repulsion of the negatively charged sulfonate groups in the case of the higher pH. At the lower pH, part of the groups are protonated, and therefore the repulsion decreases.

As it was mentioned above, we also performed simulations with a particle made of 22 PSS chains with DP = 100 each. This was performed since it is unknown what exactly the DP of PSS in the particles is, and it was interesting to clarify if the DP would have any effect on the simulation results. Additionally, it is computationally easier to model particles with several small chains instead of those with one long chain. The results (the distribution functions and electrostatic potential) for this particle model, presented in the Supplementary Information (Fig. S1), are qualitatively the same as the one chain particle model discussed here.

4.2. Zeta potential calculations

Zeta potential is defined as the electrostatic potential at the slipping (shear) plane outside a charged particle moving in an electric field where the viscous forces and the electrostatic forces are balancing each other [43]. Therefore, the zeta potential of the particle in the dispersion can in principle be approximated from the electrostatic potential profile, if the location of the slipping plane is known [43,47–49]. In general, MD simulations have been used to calculate the zeta potential based on the Helmholtz-Smoluchowski's equation for systems such as 1-palmitoyl-2-oleoyl phosphatidylcholine (POPC) bilayers, silica nanochannels, hydroxylated rutile surface, quartz surfaces, etc [47–51]. However, some studies were unable to observe the slipping plane [48,50,51] and others determined it from the average electrophoretic mobility [47]. One common feature of all MD simulation reports in this field is that they study planar surfaces and hard particles, where there is a sharp interface between the electrolyte and the surface of the particle that is impenetrable by water molecules. This makes it easy to calculate the electrophoretic mobility in water and to estimate the position of the shear plane. However, this is not the case for the present system. Therefore, we turn our attention to the fact that all the counter ions inside the slipping plane (slipping surface) move with the particle when an external electric field is applied [43]. Thus they can be thought as to be bound to the particle. Even though in our simulations we do not apply an external electric field, it is expected that this behaviour of the counter ions is still retained. In order to identify to what extent, in the radial direction, the ions are bound to the particle, we calculated the self-diffusion coefficients of Na^+ ions within shells of different radii, 0–6, 6–9, 9–12 nm and free ions not bound to any shell and therefore, free to

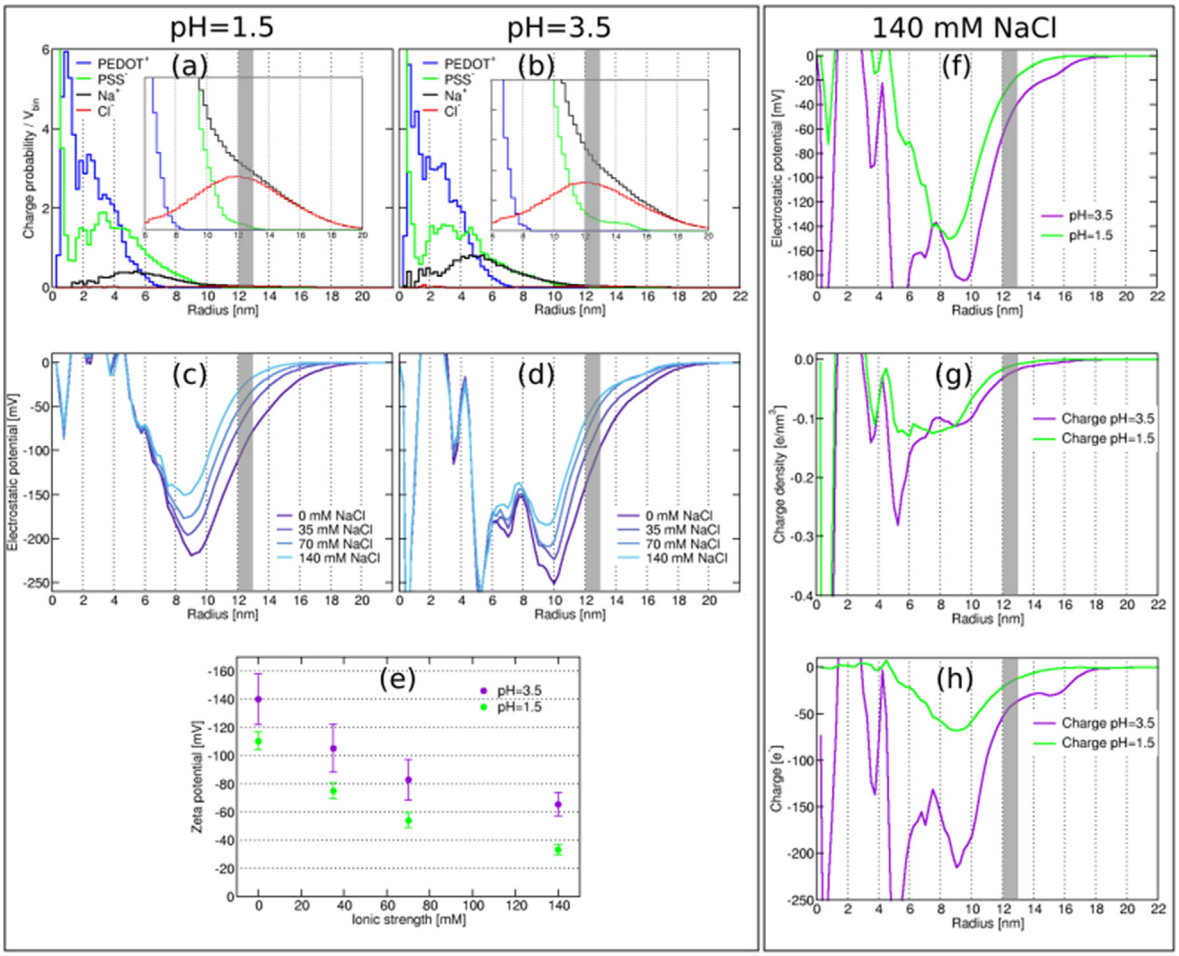

Fig. 2. Charge distribution of $PEDOT^+$, PSS^-, Na^+ and Cl^- with respect to the centre of mass of the particle for the different species for (a) pH = 1.5. (b) pH = 3.5. The insets show enlarged regions between 6 and 20 nm. The electrostatic potential in the radial direction for the particles for different ionic strength and for (c) pH = 1.5 and (d) 3.5; (e) Zeta potential of PEDOT:PSS complexes with ionic strength for different pH levels. The zeta potential corresponds to the electrostatic potential at 12 nm as explained in the text. (f) Electrostatic potential in the radial direction of the particles, (g) charge density as a function of the sphere diameter and (h) total charge in a sphere as presented in Equation (1) for the two pH = 1.5 and 3.5; the ionic strength in (f)-(g) is 140 mM NaCl. The grey regions in all plots between 12 and 13 nm show the approximated location of the slipping plane as discussed in the text.

move outside the particle beyond 12 nm (for more information see section "Self-diffusion coefficients calculations" in the SI). We compared these values with experimental results [52] and previous MD simulation of the self-diffusion coefficient performed with the MARTINI model [20] in order to compare, if there is a difference in the bulk diffusion coefficients of Na^+, with the their diffusion coefficient within the particle. In this way, we can determine if sodium ions inside the particle boundaries have reduced mobility and thus can be viewed as bound to the particle. The results are presented in Fig. 3a together with simulation snapshots (Fig. 3b) showing representative trajectories of three Na^+ ions belonging to three different shells. More information on the self-diffusion calculations can be found in the Supporting Information. Fig. 3a shows that the ions belonging to shells 0–6, 6–9 and 9–12 nm, have a much lower self-diffusion coefficient compared with the free ions (Note the logarithmic scale). Thus, we conclude that ions within 12 nm shell are bound to the particle [50], and therefore we set the slipping plane at around 12–13 nm. This is the region (highlighted in grey in Fig. 2) outside which the PSS concentration practically goes to zero. Finally, Fig. 3c presents a snapshot of a PEDOT:PSS particle with Na^+ ions within 12 nm of the COM. Hence this snapshot with ions up to 12 nm shows the particle and ions enclosed by the slipping plane.

Fig. 2g, h depicts also the total charge density and the total charge in a sphere (presented in Eq. (1)) for two pH levels considered in the simulations. It should be noted that these total charge densities include all species considered in the simulations (PEDOT, PSS, Na^+, Cl^-) except water. These distributions clearly show that the particles carry negative charge at distance up to 14–16 nm and the charge approaches zero afterwards. The total charge of the particle averaged from the region 12–13 nm (grey region in the plots) for NaCl = 0 mM is $-60e$ and $-76e$ for pH = 1.5 and 3.5, respectively, with e being the electron charge. For NaCl = 140 mM the corresponding charges are $-16e$ and $-33e$.

Fig. 2c and d presents the electrostatic potential calculated from the MD trajectories as a function of the radius of the particle and NaCl concentrations for the two pH levels used in the simulations. The grey region in the plot highlights the region discussed above and thus the value of the electrostatic potential in this region represents an approximate value of the zeta potential of the particle. It should be noted that the potential varies significantly within the particle due to many factors, e.g. limited number of particles studied, coarse-grained force field, etc. This is different from classical mean-field models and continuous representation of the systems, where fluctuations of the potential inside the particle cannot be captured [43–46].

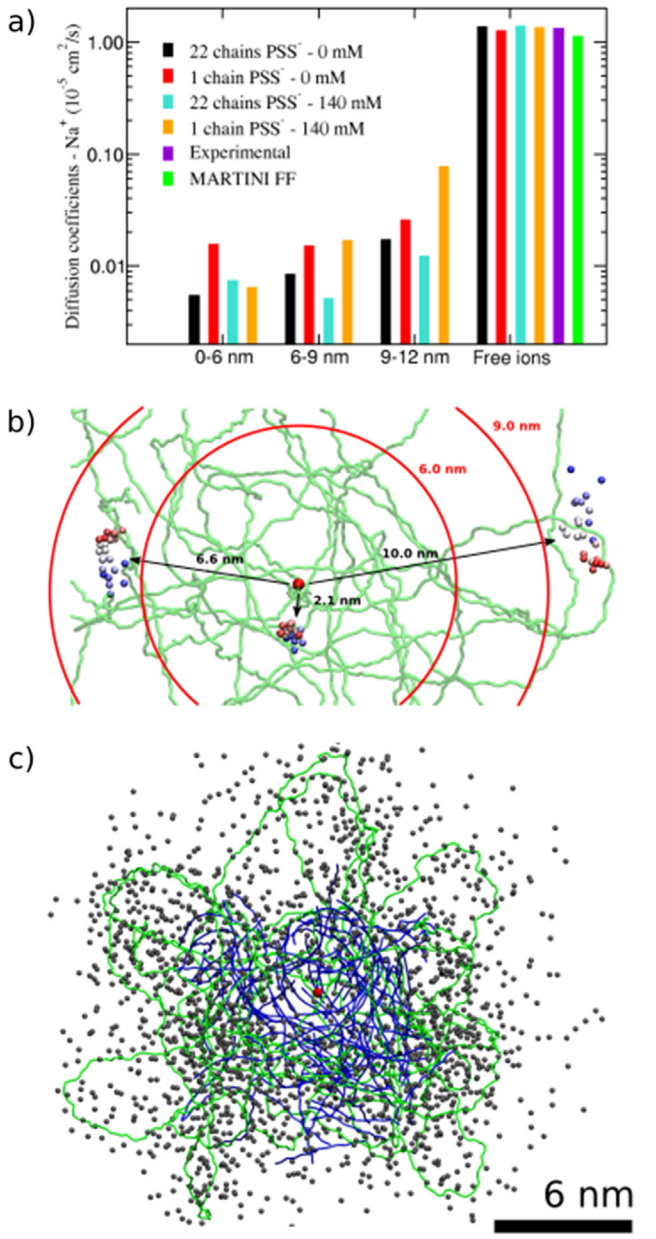

Fig. 3. (a) Self-diffusion coefficients of Na^+ as a function of the shell with given radius. The MARTINI value is taken from Reference 20 and the experimental value from Reference 52; (b) simulation snapshots of Na^+ ions trajectories occupying the shells 0–6, 6–9 and 9–12 nm, where the colour of the Na^+ ions is red in the beginning of the simulation and changes to white and finally blue at the end of the simulation. PSS chain is represented in green and the COM in a red dot in the middle; the red circles mark the extend of the shells in radial direction of the particle. (c) Snapshots showing the Na^+ ions (black) situated within 12 nm from COM. PSS is given in green, PEDOT in blue and COM in red. (For interpretation of the references to colour in this figure legend, the reader is referred to the web version of this article.)

It is interesting to note the changes in the electrostatic potential at different pH and ionic strengths. At the lower pH, the negative potential reaches less negative values, i.e. −200 mV, which is the minimum of the potential curves at 9 nm compared to the higher pH value of −250 mV where also the minimum is shifted to 10 nm, as seen from Fig. 2c, d. It can be also noted that there is another minimum in the potential at 5 nm for pH = 3.5. This minimum represents large fluctuations of the potential inside the particle as discussed in the previous paragraph. As the salt concentration is increased the absolute value of the negative potential becomes lower and the smaller the charge of the PSS (i.e. higher pH), the larger is the effect. This is also be expected from the mean-field approximations but apparently our present molecular dynamics simulations provide much more microscopic details concerning atomistic organization of PEDOT:PSS complexes [53–55].

It is evident from Fig. 2c and d, that the potential after reaching the minimum at 9 and 10 nm for pH = 1.5 and 3.5, respectively, gradually decreases to zero. For pH = 3.5, the electrostatic potential at 12 nm (approximate location of the slipping plane) alters between −140 mV to −65 mV for NaCl concentrations of 0 to 140 mM, respectively. At 13 nm, the potential is found to fall in the range between −95 mV and −40 mV, with the increase of the ionic strength. Theoretically it is expected that the absolute value of the zeta potential should decrease with the increase of the ionic strength which is well captured by our simulations and the change in our estimated zeta potential is shown in Fig. 2e [43,51]. In simplified terms this decrease is due to the screening of the particle charge from the surrounding electrolyte.

4.3. Investigation of particle size using DLS

The particle size of PEDOT:PSS was measured experimentally with DLS. Fig. 4a shows the volume and intensity size distribution of PEDOT:PSS particles at pH 3.5. The corresponding size distribution for undialyzed and unfiltered PEDOT:PSS solution at pH 3.5 is shown in Fig. S5a. As can be seen, the larger aggregates in the volume distribution has been removed, providing a cleaner PEDOT:PSS solution.

The volume distribution shows that the majority of the complexes are within 16 nm, and that there is only a small fraction of particles that are 30 nm or larger. On the other hand, the intensity distribution shows that the majority of the complexes have a diameter >100 nm and a lower fraction is below 30 nm. This dissimilarity in particle size is inherent to how the size distribution is evaluated from the autocorrelation function. For the intensity distribution, the amount of light scattered by particles is converted to particle size using Stokes-Einstein equation. However, according to the Rayleigh approximation, larger particles scatter more light ($I \propto d^6$, d is diameter of particle) which means that the presence of even small fractions of large particles in the dispersion create a large contribution to the intensity distribution. From the volume distribution (calculated from intensity distribution using Mie theory) [56,57], it can also be concluded that there is a small fraction of complexes in this size range. Hence, for further analysis of the results and for comparison to the theoretical evaluation, only the volume size distribution will be used. The use of the volume distribution is also a standard procedure for the evaluation of DLS data for predicting the change in average particle size and its changes with solution properties.

The reported size of PEDOT:PSS complexes before and after modification, with added secondary dopants, is usually in the range between 30 nm and 1 μm [12–14,58]. However, for the cleaned complexes studied in the present work, it is indeed observed that PEDOT:PSS particles are within 16 nm in diameter. Similar values were also reported in some earlier studies, where, PEDOT:PSS films displayed spherical complexes between 15 and 20 nm, as investigated by using WAXS, SAXS, AFM and STM [7,59,60].

The pH and ionic strength of PEDOT: PSS complex dispersion were altered in order to study their effect on the particle size distribution. It can be seen in Fig. 4b that changing pH from 3.5 to 1.7, i.e. addition of acid, shifts the particle size to lower values. The majority particles at pH 1.7 are within the range of 12 nm, whereas, at pH 3.5 it was 16 nm which was expected due to the lower charge of the PSS at the lower pH. The experimentally measured particle size at pH 1.7 and 3.5 agrees well with the trends

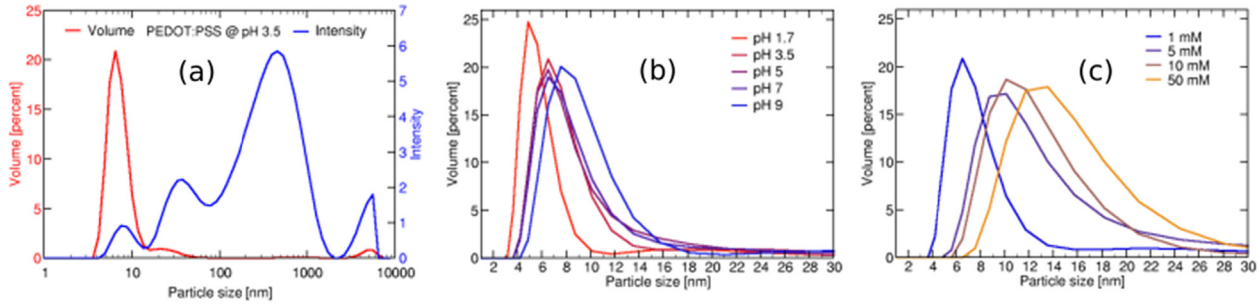

Fig. 4. The size distribution (presented as diameter) of PEDOT:PSS particles by (a) volume and intensity, measured at pH 3.5 (1 mM NaCl) using DLS; The size distribution by volume for PEDOT:PSS particles at different (b) pH (1 mM NaCl), and (c) ionic strength (pH 3.5).

observed in the simulated PEDOT:PSS particle at the respective pH levels (Fig. 2a and 2b, respectively). The pH of system was further increased experimentally to study the change in particle size. The size does not change from pH 3.5 to 7, as the change in pH from 3.5 to 7 only demands a minor increase in ionic strength due to the addition of NaOH and this will not affect the stability of the PEDOT:PSS particles since PSS is fully charged in this pH-regime. However, an increase to 19 nm was observed at pH 9. Similarly, by changing the ionic strength from 1 mM to 5 mM, the change in particle size is significant, from 16 nm to 28 nm (Fig 4c), whereas the particle size increases slightly to 30 nm at 10 mM and 38 nm at 50 mM ionic strength. Please note that only the major peaks for particle size is shown in Fig. 4b,c since there are very few aggregates with larger diameters, as described earlier. For complete data please refer to Fig. S5 in supplementary information.

There can be several reasons for observed trend in particle size with changing pH. At pH 1.7, proton is a counterion to PSS and some of the charged groups on PSS will be in their protonated form, which will lead to a lower interaction between the PEDOT and the PSS. Due to the significantly increased concentration of the Cl^- at the lower pH, there is also a possibility that some of the counterions to $PEDOT^+$ might be exchanged to Cl^- from bulky PSS^-. All these effects would lead to a decrease in the overall particle size, which is seen both in simulations and experiments. A decrease in pH to pH = 1.7 also results in an increase in ionic strength of the dispersion which will affect the interaction between the particles and the interactions between PSS chains on the surface of the complexes leading to a lower extension of the PSS chains and a smaller size of the complexes. The decreased repulsion between the complexes could lead to an association of the complexes to larger aggregates. As demonstrated in Fig. 4b the first process is most probably the dominating process. As the pH is increased to 9, the counterion to PSS^- are changed from proton to sodium and the PEDOT component of the complex will also achieve a lower charge due to de-doping of PEDOT:PSS [61]. An increase of the pH to 9 is also equivalent to an increased ionic strength which will lead to a lower repulsion between PEDOT:PSS complexes allowing for complex association. Both these effects will hence lead to an increase in size of the complex. However, an increased ionic strength will also, as mentioned earlier, lead to a decreased expansion of the PSS in the outer layer of the complex, so the overall diameter of the complex will be given by a balance of the interactions within the core of the complex, the extension of the PSS chains and a more macroscopic association of the complexes. The changes in dimensions of the complexes with changes in ionic strength most probably have the same fundamental explanations as those behind the dimensional changes found with changes in pH.

The effect of changes in pH and alkali metal salt concentrations on the conductive properties of the PEDOT:PSS films has previously been investigated, and as pH and alkali metal concentration was increased to higher values, the electrical conductivity of PEDOT:PSS films was decreased [16,62]. Different mechanisms were proposed for such behaviour. As was mentioned earlier, de-doping of PEDOT:PSS at pH > 7 or at high Na^+ concentration was proposed by Kok et al. [61] Similar studies were conducted by Mochizuki et al. [15] using a pH range between pH = 1.7 to pH = 12 and by using conductive AFM, they observed a decrease in size and the number of conductive domains as the pH is increased. The present results show that an understanding and control of the changes in the dispersion properties of the PEDOT:PSS complexes during the preparation of the conductive polymer films is crucial for an efficient use of intrinsic properties of PEDOT:PSS. Since, most films are prepared by some film-casting technique where increases in the ionic strength and/or changes in pH will occur as the solvent is removed. For that reason, the model developed in this study for simulating PEDOT:PSS particles and careful sample preparations for the DLS experiments, paves a way forward to understand the complicated and dynamic PEDOT:PSS complexes in dispersion.

4.4. Zeta potential measured with DLS

The trends in zeta potential with changing pH and ionic strength as measured with DLS, is shown in Fig. 5 (a, b), respectively. The measured values are between −50 mV to −30 mV with an increasing pH from 3.5 to 9 and is decreased to −30 mV when the pH is lowered to 1.7. The results also show that the zeta potential decreased from −50 mV to −30 mV with increasing ionic strength from 1 mM to 10 mM and again increased to −39 mV at 50 mM NaCl.

As additional information to the zeta-potential measurements, the charge density of PEDOT:PSS was measured by titrating the complex with PDADMAC, a positively charged polymer. The trend in charge density with changing pH of the PEDOT:PSS solution is shown in Fig. 5c. From the figure, it is obvious that the charge density shows a maximum at pH = 3.5 (2000μeq/g) and it is still high at pH = 1.7 (1800μeq/g) and pH = 9 (1500μeq/g). As is commonly known, a high surface charge of the particles will lead to a high electrostatic repulsion creating a colloidally stable particle dispersion. This rather high negative charge density over the entire pH-range can explain the significant colloidal stability of PEDOT:PSS complexes. To be consistent with the experiments, we calculated the total charge of the particle considering only the excess charges from the PSS chains from the simulations, which is found to be 1.8×10^3 charges/particle (calculated from DP = 2200 for PSS and DP = 12 for PEDOT and pH = 3.5). To compare calculated and experimental results, we converted μeq/g to charge /particle. However, in experiments, the charge density is the number of charges titrated with PDADMAC and with the colloidal titration technique only the charges emanating from the PSS can be determined [63]. It should also be noted that only the surface charges

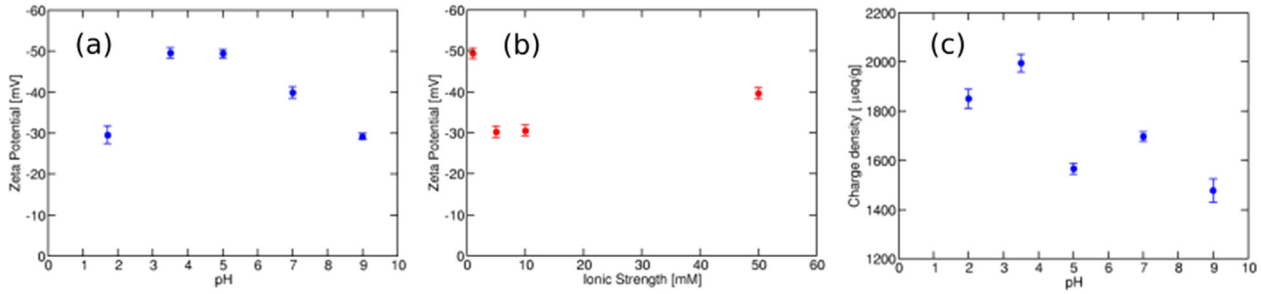

Fig. 5. The change in zeta potential with (a) pH (1 mM NaCl), and (b) ionic strength (pH 3.5), as measured using DLS; (c) charge density of PEDOT:PSS at different pH (in 1 mM NaCl) measured using polyelectrolyte titration.

from PSS chain are available to PDADMAC. Considering the density of PEDOT:PSS as 1000 Kg/m^3, the mass obtained for 16 nm PEDOT:PSS particle is 2.58 $\times$ 10^{-18} g/particle. From the charge density measurements it is known that the charge is 2 $\times$ 10^{-3} mole charges/g. This will result into 4.28 $\times$ 10^{-21} mole charges/particle and after multiplying with N_A (Avogadro number; 6.023 $\times$ 10^{23}) charges/mole), we obtain 2.58 $\times$ 10^3 charges/particle. This value is very similar to the charge density of 1.8 $\times$ 10^3 obtained from MD simulations. The difference in values could arise due to the assumed density of PEDOT:PSS particles. The density of PEDOT:PSS aqueous dispersion (1.3 wt%) as provided by supplier is 1000 Kg/m^3 which was measured on films and therefore, the density of aqueous dispersion is not known. As the particle size in dispersion, i.e. 16 nm, is very similar to the particle size in thin films, i.e. 13 nm [17], the density of 1000 Kg/m^3 in aqueous dispersion is a good approximation. However, one should note that these are just theoretical assumptions and are described here to explain the differences and difficulties involved in comparing simulated and experimental values of charge density. Nevertheless, the simulated charge density shows similar trend as in the experiments, i.e. increase of the charge with the pH for these two pH levels.

The change of the surface charge of the complexes must also be considered when evaluating the changes in the zeta-potential of the complexes, since there indeed is a connection between charge and potential, i.e. for a simple inert colloid, an increased surface charge leads to a higher surface potential and hence also zeta potential. By comparing Fig. 5a and 5c, similar shape of the curves can be detected. The reason to the lower charge at pH = 1.5 is naturally a protonation of the PSS and the decrease of the charge above pH = 3.5 can most probably be linked to the balance between the charges of the PEDOT and the PSS which is an intricate balance. Apart from the influence of the charge, the dimensions of the complexes and the extension of the PSS from the complex surface will naturally lead to a change of the slipping plane used for determining the zeta potential. The decrease of the pH will also lead to an increase in ionic strength which in turn will lower the surface potential and also the zeta potential. This can also explain the decrease of the zeta potential with increasing salt concentrations. However, the increase in zeta potential at the highest salt concentration is more difficult to explain. Since the pH for these measurements is around pH = 3.5 and a change in the salt concentration can both lead to a somewhat increased charge of the PSS due to an increase pH inside the complex due to the Donnan effect and a decrease of the extension of the PSS outside the complex. This could explain the detected results, but these speculations should be studied more in detail in future, using a combination of simulations and experimental investigations.

Finally, remarks are in order, on the comparison between the experimental and simulation results. Throughout the discussion of the results, we show that the experimental and simulation results qualitatively agree with each other and the trends of the measured properties (particle size, zeta potential and particle charge) are well matched. However, a couple of clarifications regarding this comparison need to be added.

In order to construct an accurate molecular model of PEDOT:PSS particle, it is necessary to have information about the number of molecules and degree of polymerisation of the constituents in the single particle. However, such experimental data is not available, especially for widely used commercial samples. Moreover, there is a distribution of these numbers rather than a single value. As we mentioned earlier, we did not have *a priori* knowledge what the particle size would be with this particular number of molecules used to create the particles. Thus, obtaining and simulating a specific particle size is demanding and tedious work not intended to be done in this study, since this is not the focus in here. Therefore, the particle size in the simulations (~25 nm) and in the experiments (>16 nm) differs by its absolute value. The larger size in the simulations is most likely due to the larger number of molecules (or longer PSS chains) used to prepare them compared to experimental ones. Obviously, there is not a direct way to extract the number of molecules in a particle by experiments, and therefore the choice of this number in the simulations can be overestimated, which results in a larger particle. However, indirectly from the experiments, we can approximate the number of molecules in a particle in conjunction with the simulations by altering this number and simulating and calculating the size. This iterative work was not intended in the present study.

The number of molecules in the particles (size of particle) might also affect the calculated zeta potential. By keeping the PEDOT to PSS ratio (1:2.5) but increasing the particle size (number of molecules in particle), the surface charge density of the particles might be increased. This would lead to an increase of the calculated zeta potential observed in our work.

Nevertheless, the relative changes of the particle size, zeta potential and charge density with variations of the pH and ionic strength are in good agreement between the simulations and experiments.

5. Conclusion

In this study, MARTINI coarse grained force field model was used to simulate PEDOT:PSS particles in dispersion, calculate the zeta potential and the particle size, and obtain the distribution of $PEDOT^+$, PSS^-, Na^+ and Cl^- in the particles. Dynamic light scattering (DLS) technique was used to measure particle size and zeta potential experimentally and both investigations were made independent of each other, without fitting the experimental data in the simulations. The simulations as well as DLS measurements show a decrease in the particle dimensions with decreasing pH level

from 3.5 to 1.7. When the pH was further increased to 9 in the experiments, the particles become even larger. Similarly, by changing the ionic strength, the dimensions of the complex are significantly changed. The charge density of PEDOT:PSS complexes measured with polyelectrolyte titration was also in agreement with simulated values. The zeta potential of simulated particles shows the same trend with changing pH and ionic strength, and the simulated and the measured values are in good agreement. Even though the simulations were performed in parallel, without the knowledge of results from experiments, the particle size, z-potential and charge density agree qualitatively well. Therefore, we are convinced that this study will help in further understanding of PEDOT:PSS particles in dispersion which is otherwise difficult to simulate, and the combination of experimental and theoretical investigations provides a new, general and efficient tool for understanding of polyelectrolyte complex formation. In future, the interaction of PEDOT:PSS with other polymers such as cellulose can be modelled using this study to understand the system at molecular level and to prepare better nanocomposites.

CRediT authorship contribution statement

Karishma Jain: Conceptualization, Methodology, Validation, Formal analysis, Investigation, Data curation, Writing - original draft, Visualization, Writing - review & editing. **Aleksandar Y. Mehandzhiyski:** Conceptualization, Methodology, Software, Validation, Formal analysis, Investigation, Data curation, Writing - original draft, Visualization, Writing - review & editing. **Igor Zozoulenko:** Conceptualization, Writing - original draft, Supervision, Resources, Funding acquisition, Project administration, Writing - review & editing. **Lars Wågberg:** Conceptualization, Writing - original draft, Supervision, Resources, Funding acquisition, Project administration, Writing - review & editing.

Declaration of Competing Interest

The authors declare that they have no known competing financial interests or personal relationships that could have appeared to influence the work reported in this paper.

Acknowledgements

KJ acknowledges Vinnova through the Digital Cellulose Centre for financial support. AYM acknowledges Treesearch for financial support. LW and IZ acknowledge the Wallenberg Wood Science Centre for financial support. IZ thanks the Advanced Functional Material Center at Linköping University for support. The computations were performed on resources provided by the Swedish National Infrastructure for Computing (SNIC) at NSC and HPC2N.

Appendix A. Supplementary material

Supplementary data to this article can be found online at https://doi.org/10.1016/j.jcis.2020.09.070.

References

[1] M. Berggren, X. Crispin, S. Fabiano, M.P. Jonsson, D.T. Simon, E. Stavrinidou, K. Tybrandt, I. Zozoulenko, Ion electron-coupled functionality in materials and devices based on conjugated polymers, Adv. Mater. 31 (22) (2019) 1805813, https://doi.org/10.1002/adma.201805813.
[2] K. Sun, S. Zhang, P. Li, Y. Xia, X. Zhang, D. Du, F.H. Isikgor, J. Ouyang, Review on application of PEDOTs and PEDOT:PSS in energy conversion and storage devices, J. Mater. Sci.: Mater. Electron. 26 (7) (2015) 4438–4462, https://doi.org/10.1007/s10854-015-2895-5.
[3] Y. Wen, J. Xu, Scientific importance of water-processable PEDOT–PSS and preparation, challenge and new application in sensors of its film electrode: a review, J. Polym. Sci., Part A: Polym. Chem. 55 (7) (2017) 1121–1150, https://doi.org/10.1002/pola.28482.
[4] G. Greczynski, T. Kugler, M. Keil, W. Osikowicz, M. Fahlman, W.R. Salaneck, Photoelectron spectroscopy of thin films of PEDOT–PSS conjugated polymer blend: a mini-review and some new results, J. Electron Spectrosc. Relat. Phenom. 121 (1) (2001) 1–17, https://doi.org/10.1016/S0368-2048(01)00323-1.
[5] T. Horii, Y. Li, Y. Mori, H. Okuzaki, Correlation between the hierarchical structure and electrical conductivity of PEDOT/PSS, Polym. J. 47 (10) (2015) 695–699, https://doi.org/10.1038/pj.2015.48.
[6] Q. Wei, M. Mukaida, Y. Naitoh, T. Ishida, Morphological change and mobility enhancement in PEDOT:PSS by adding co-solvents, Adv. Mater. 25 (20) (2013) 2831–2836, https://doi.org/10.1002/adma.201205158.
[7] T. Takano, H. Masunaga, A. Fujiwara, H. Okuzaki, T. Sasaki, PEDOT nanocrystal in highly conductive PEDOT:PSS polymer films, Macromolecules 45 (9) (2012) 3859–3865, https://doi.org/10.1021/ma300120g.
[8] X. Crispin, F.L.E. Jakobsson, A. Crispin, P.C.M. Grim, P. Andersson, A. Volodin, C. van Haesendonck, The origin of the high conductivity of poly(3,4-ethylenedioxythiophene)-poly(styrenesulfonate) (PEDOT-PSS) plastic electrodes. 7.
[9] A.M. Nardes, M. Kemerink, R.a.J. Janssen, J.A.M. Bastiaansen, N.M.M. Kiggen, B. M.W. Langeveld, A.J.J.M. van Breemen, M.M. de Kok, Microscopic understanding of the anisotropic conductivity of PEDOT:PSS thin films, Adv. Mater. 19 (9) (2007) 1196–1200, https://doi.org/10.1002/adma.200602575.
[10] S. Timpanaro, M. Kemerink, F.J. Touwslager, M.M. De Kok, S. Schrader, Morphology and conductivity of PEDOT/PSS films studied by scanning-tunneling microscopy, Chem. Phys. Lett. 394 (4) (2004) 339–343, https://doi.org/10.1016/j.cplett.2004.07.035.
[11] L. Ouyang, C. Musumeci, M.J. Jafari, T. Ederth, O. Inganäs, Imaging the phase separation between PEDOT and polyelectrolytes during processing of highly conductive PEDOT:PSS films, ACS Appl. Mater. Interfaces 7 (35) (2015) 19764–19773, https://doi.org/10.1021/acsami.5b05439.
[12] Z. Fan, D. Du, H. Yao, J. Ouyang, Higher PEDOT molecular weight giving rise to higher thermoelectric property of PEDOT:PSS: A comparative study of clevios P and clevios PH1000, ACS Appl. Mater. Interfaces 9 (13) (2017) 11732–11738, https://doi.org/10.1021/acsami.6b15158.
[13] Y. Xu, P.A. Patsis, S. Hauser, D. Voigt, R. Rothe, M. Günther, M. Cui, X. Yang, R. Wieduwild, K. Eckert, C. Neinhuis, T.F. Akbar, I.R. Minev, J. Pietzsch, Y. Zhang, Cytocompatible, injectable, and electroconductive soft adhesives with hybrid covalent/noncovalent dynamic network, Adv. Sci. 6 (15) (2019) 1802077, https://doi.org/10.1002/advs.201802077.
[14] M. Horikawa, T. Fujiki, T. Shirosaki, N. Ryu, H. Sakurai, S. Nagaoka, H. Ihara, The development of a highly conductive PEDOT system by doping with partially crystalline sulfated cellulose and its electric conductivity, J. Mater. Chem. C 3 (34) (2015) 8881–8887, https://doi.org/10.1039/C5TC02074C.
[15] Y. Mochizuki, T. Horii, H. Okuzaki, Effect of PH on structure and conductivity of PEDOT/PSS, Trans. Mat. Res. Soc. Japan 37 (2) (2012) 307–310, https://doi.org/10.14723/tmrsj.37.307.
[16] F. Kong, C. Liu, H. Song, J. Xu, Y. Huang, H. Zhu, J. Wang, Effect of solution PH value on thermoelectric performance of free-standing PEDOT:PSS films, Synth. Met. 185–186 (2013) 31–37, https://doi.org/10.1016/j.synthmet.2013.09.046.
[17] D. Belaineh, J.W. Andreasen, J. Palisaitis, A. Malti, K. Håkansson, L. Wågberg, X. Crispin, I. Engquist, M. Berggren, Controlling the organization of PEDOT:PSS on cellulose structures, ACS Appl. Polym. Mater. 1 (9) (2019) 2342–2351, https://doi.org/10.1021/acsapm.9b00444.
[18] A. Malti, J. Edberg, H. Granberg, Z.U. Khan, J.W. Andreasen, X. Liu, D. Zhao, H. Zhang, Y. Yao, J.W. Brill, I. Engquist, M. Fahlman, L. Wågberg, X. Crispin, M. Berggren, An organic mixed ion-electron conductor for power electronics, Adv. Sci. 3 (2) (2016) 1500305, https://doi.org/10.1002/advs.201500305.
[19] Z.U. Khan, J. Edberg, M.M. Hamedi, R. Gabrielsson, H. Granberg, L. Wågberg, I. Engquist, M. Berggren, X. Crispin, Thermoelectric polymers and their elastic aerogels, Adv. Mater. 28 (22) (2016) 4556–4562, https://doi.org/10.1002/adma.201505364.
[20] M. Modarresi, J. Felipe Franco-Gonzalez, I. Zozoulenko, Morphology and ion diffusion in PEDOT:Tos. A coarse grained molecular dynamics simulation, PCCP 20 (25) (2018) 17188–17198, https://doi.org/10.1039/C8CP02902D.
[21] J.F. Franco-Gonzalez, I.V. Zozoulenko, Molecular dynamics study of morphology of doped PEDOT: From solution to dry phase, J. Phys. Chem. B 121 (16) (2017) 4299–4307, https://doi.org/10.1021/acs.jpcb.7b01510.
[22] D. Kim, I. Zozoulenko, Why is pristine PEDOT oxidized to 33%? A density functional theory study of oxidative polymerization mechanism, J. Phys. Chem. B 123 (24) (2019) 5160–5167, https://doi.org/10.1021/acs.jpcb.9b01745.
[23] M. Modarresi, J. Felipe Franco-Gonzalez, I. Zozoulenko, Computational microscopy study of the granular structure and PH dependence of PEDOT:PSS, PCCP 21 (12) (2019) 6699–6711, https://doi.org/10.1039/C8CP07141A.
[24] M. Modarresi, A. Mehandzhiyski, M. Fahlman, K. Tybrandt, I. Zozoulenko, Microscopic understanding of the granular structure and the swelling of PEDOT:PSS, Macromolecules 53 (15) (2020) 6267–6278, https://doi.org/10.1021/acs.macromol.0c00877.
[25] S.J. Marrink, H.J. Risselada, S. Yefimov, D.P. Tieleman, A.H. de Vries, The MARTINI force field: coarse grained model for biomolecular simulations, J. Phys. Chem. B 111 (27) (2007) 7812–7824, https://doi.org/10.1021/jp071097f.
[26] M. Vögele, C. Holm, J. Smiatek, Coarse-grained simulations of polyelectrolyte complexes: MARTINI models for poly(styrene sulfonate) and poly

(diallyldimethylammonium) 243151, J. Chem. Phys. 143 (24) (2015), https://doi.org/10.1063/1.4937805.
[27] A. Elschner, S. Kirchmeyer, W. Lovenich, U. Merker, K. Reuter, S. Kirchmeyer, W. Lovenich, U. Merker, K. Reuter, PEDOT : Principles and Applications of an Intrinsically Conductive Polymer, CRC Press (2010), https://doi.org/10.1201/b10318.
[28] S.O. Yesylevskyy, L.V. Schäfer, D. Sengupta, S.J. Marrink, Polarizable water model for the coarse-grained MARTINI force field e1000810, PLoS Comput. Biol. 6 (6) (2010), https://doi.org/10.1371/journal.pcbi.1000810.
[29] T. Horii, H. Hikawa, Y. Mochizuki, H. Okuzaki, Synthesis and characterization of highly conductive PEDOT/PSS colloidal gels, Trans. Mat. Res. Soc. Japan 37 (4) (2012) 515–518. 10.14723/tmrsj.37.515.
[30] T.A. Skotheim, J. Reynolds, J. Reynolds, Conjugated Polymers: Theory, Synthesis, Properties, and Characterization, CRC Press (2006), https://doi.org/10.1201/9781420043594.
[31] P.O. Danis, D.E. Karr, Analysis of poly(styrenesulfonic acid) by matrix-assisted laser desorption/ionization time-of-flight mass spectrometry, Macromolecules 28 (25) (1995) 8548–8551, https://doi.org/10.1021/ma00129a013.
[32] B.N. Dickhaus, R. Priefer, Determination of polyelectrolyte PKa values using surface-to-air tension measurements, Colloids Surf. A 488 (2016) 15–19, https://doi.org/10.1016/j.colsurfa.2015.10.015.
[33] H.J.C. Berendsen, J.P.M. Postma, W.F. van Gunsteren, A. DiNola, J.R. Haak, Molecular dynamics with coupling to an external bath, J. Chem. Phys. 81 (8) (1984) 3684–3690, https://doi.org/10.1063/1.448118.
[34] G. Bussi, D. Donadio, M. Parrinello, Canonical sampling through velocity rescaling 014101, J. Chem. Phys. 126 (1) (2007), https://doi.org/10.1063/1.2408420.
[35] U. Essmann, L. Perera, M.L. Berkowitz, T. Darden, H. Lee, L.G. Pedersen, A smooth particle mesh Ewald method, J. Chem. Phys. 103 (19) (1995) 8577–8593, https://doi.org/10.1063/1.470117.
[36] M.J. Abraham, T. Murtola, R. Schulz, S. Páll, J.C. Smith, B. Hess, E. Lindahl, GROMACS: high performance molecular simulations through multi-level parallelism from laptops to supercomputers, SoftwareX 1–2 (2015) 19–25, https://doi.org/10.1016/j.softx.2015.06.001.
[37] W. Humphrey, A. Dalke, K. Schulten, VMD: visual molecular dynamics, J. Mol. Graph. 14 (1) (1996) 33–38, https://doi.org/10.1016/0263-7855(96)00018-5.
[38] N. Michaud-Agrawal, E.J. Denning, T.B. Woolf, O. Beckstein, MDAnalysis: A toolkit for the analysis of molecular dynamics simulations, J. Comput. Chem. 32 (10) (2011) 2319–2327, https://doi.org/10.1002/jcc.21787.
[39] R. Gowers, M. Linke, J. Barnoud, T. Reddy, M. Melo, S. Seyler, J. Domański, D. Dotson, S. Buchoux, I. Kenney, O. Beckstein, MDAnalysis: A python package for the rapid analysis of molecular dynamics simulations; Austin, Texas (2016) 98–105, https://doi.org/10.25080/Majora-629e541a-00e.
[40] G.S. Anderson, R.C. Miller, A.R.H. Goodwin, Static dielectric constants for liquid water from 300 K to 350 K at pressures to 13 MPa using a new radio-frequency resonator, J. Chem. Eng. Data 45 (4) (2000) 549–554, https://doi.org/10.1021/je9903092.
[41] A.Y. Mehandzhiyski, I. Zozoulenko, Computational microscopy of PEDOT:PSS/cellulose composite paper, ACS Appl. Energy Mater. 2 (5) (2019) 3568–3577, https://doi.org/10.1021/acsaem.9b00307.
[42] H.I. Ingólfsson, C. Arnarez, X. Periole, S.J. Marrink, Computational 'microscopy' of cellular membranes, J. Cell Sci. 129 (2) (2016) 257–268, https://doi.org/10.1242/jcs.176040.
[43] G.V. Lowry, R.J. Hill, S. Harper, A.F. Rawle, C.O. Hendren, F. Klaessig, U. Nobbmann, P. Sayre, J. Rumble, Guidance to improve the scientific value of zeta-potential measurements in NanoEHS, Environ. Sci. Nano 3 (5) (2016) 953–965, https://doi.org/10.1039/C6EN00136J.
[44] H. Ohshima, Theory of electrostatics and electrokinetics of soft particles 063001, Sci. Technol. Adv. Mater. 10 (6) (2009), https://doi.org/10.1088/1468-6996/10/6/063001.
[45] H. Ohshima, Electrical phenomena in a suspension of soft particles, Soft Matter 8 (13) (2012) 3511–3514, https://doi.org/10.1039/C2SM07160F.
[46] H. Ohshima, Electrokinetic phenomena of soft particles, Curr. Opin. Colloid Interface Sci. 18 (2) (2013) 73–82, https://doi.org/10.1016/j.cocis.2013.02.003.
[47] V. Knecht, B. Klasczyk, R. Dimova, Macro- versus microscopic view on the electrokinetics of a water-membrane interface, Langmuir 29 (25) (2013) 7939–7948, https://doi.org/10.1021/la400342m.
[48] Z. Brkljača, D. Namjesnik, J. Lützenkirchen, M. Předota, T. Preočanin, Quartz/aqueous electrolyte solution interface: molecular dynamic simulation and interfacial potential measurements, J. Phys. Chem. C 122 (42) (2018) 24025–24036, https://doi.org/10.1021/acs.jpcc.8b04035.
[49] A. Gupta, S. Vasudevan, Understanding surfactant stabilization of MoS2 nanosheets in aqueous dispersions from zeta potential measurements and molecular dynamics simulations, J. Phys. Chem. C 122 (33) (2018) 19243–19250, https://doi.org/10.1021/acs.jpcc.8b05922.
[50] B. Siboulet, S. Hocine, R. Hartkamp, J.-F. Dufrêche, Scrutinizing electro-osmosis and surface conductivity with molecular dynamics, J. Phys. Chem. C 121 (12) (2017) 6756–6769, https://doi.org/10.1021/acs.jpcc.7b00309.
[51] M. Předota, M.L. Machesky, D.J. Wesolowski, Molecular origins of the zeta potential, Langmuir 32 (40) (2016) 10189–10198, https://doi.org/10.1021/acs.langmuir.6b02493.
[52] E. Samson, J. Marchand, K.A. Snyder, Calculation of ionic diffusion coefficients on the basis of migration test results, Mater. Struct. 36 (2003) 10.
[53] P.-G. de Gennes, Some conformation problems for long macromolecules, Rep. Prog. Phys. 32 (1) (1969) 187–205, https://doi.org/10.1088/0034-4885/32/1/304.
[54] P.G. De Gennes, Polymer solutions near an interface. Adsorption and depletion layers, Macromolecules 14 (6) (1981) 1637–1644, https://doi.org/10.1021/ma50007a007.
[55] G.H. Fredrickson, H. Orland, Dynamics of polymers: a mean-field theory 084902, J. Chem. Phys. 140 (8) (2014), https://doi.org/10.1063/1.4865911.
[56] G. Mie, Beiträge Zur Optik Trüber Medien, Speziell Kolloidaler Metallösungen, Ann. Phys. 330 (3) (1908) 377–445, https://doi.org/10.1002/andp.19083300302.
[57] J. Stetefeld, S.A. McKenna, T.R. Patel, Dynamic light scattering: a practical guide and applications in biomedical sciences, Biophys. Rev. 8 (4) (2016) 409–427, https://doi.org/10.1007/s12551-016-0218-6.
[58] G.-F. Wang, X.-M. Tao, J.H. Xin, B. Fei, Modification of conductive polymer for polymeric anodes of flexible organic light-emitting diodes, Nanoscale Res. Lett. 4 (7) (2009) 613–617, https://doi.org/10.1007/s11671-009-9288-8.
[59] H. Yan, S. Arima, Y. Mori, T. Kagata, H. Sato, H. Okuzaki, Poly(3,4-ethylenedioxythiophene)/poly(4-styrenesulfonate): correlation between colloidal particles and thin films, Thin Solid Films 517 (11) (2009) 3299–3303, https://doi.org/10.1016/j.tsf.2009.01.004.
[60] M. Kemerink, S. Timpanaro, M.M. de Kok, E.A. Meulenkamp, F.J. Touwslager, Three-dimensional inhomogeneities in PEDOT:PSS films, J. Phys. Chem. B 108 (49) (2004) 18820–18825, https://doi.org/10.1021/jp0464674.
[61] M.M. de Kok, M. Buechel, S.I.E. Vulto, P. van de Weijer, E.A. Meulenkamp, S.H.P. M. de Winter, A.J.G. Mank, H.J.M. Vorstenbosch, C.H.L. Weijtens, V. van Elsbergen, Modification of PEDOT:PSS as hole injection layer in polymer LEDs. Physica Status Solidi (a) 2004, 201 (6), 1342–1359. https://doi.org/10.1002/pssa.200404338
[62] C.H.L. Weijtens, V. van Elsbergen, M.M. de Kok, S.H.P.M. de Winter, Effect of the alkali metal content on the electronic properties of PEDOT:PSS, Org. Electron. 6 (2) (2005) 97–104, https://doi.org/10.1016/j.orgel.2005.02.005.
[63] D. Horn, in: E.J. Goethals (Ed.), Polymeric Amines and Ammonium Salts, Pregman Press: New York, 1980, pp 333–355.